Penerbit Akademia Baru

Journal of Advanced Research in Micro and Nano Engineering

Journal homepage:
https://www.akademiabaru.com/submit/index.php/armne/index
ISSN: 2756-8210

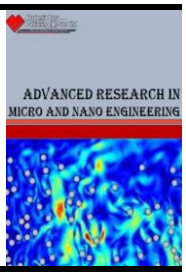

Fabrication and Characterization of Nanocoils CNT/PLA Filament at Different Filler's Percentages as Electromagnetic Wave Absorbers

Farah Hamizah Puad@Paat[1,2], Nawrah Afnan Ashraf[1,2], Fadzidah Mohd Idris[1,*]

[1] Kolej PERMATA Insan, Universiti Sains Islam Malaysia, Bandar Baru Nilai, 71800 Nilai, Negeri Sembilan, Malaysia
[2] Energy Materials Research Consortium, Faculty of Science and Technology, Universiti Sains Islam Malaysia, 71800, Nilai, Negeri Sembilan, Malaysia

ARTICLE INFO

Article history:
Received 10 January 2024
Received in revised form 28 February 2024
Accepted 17 April 2024
Available online 30 May 2024

Keywords:
EMI pollution; carbon nanocomposites; fillers; reflection loss; 3D printing

ABSTRACT

The rapid development of electronic technology and communication networks has resulted in high levels of electromagnetic interference (EMI) pollution, indirectly making electromagnetic wave (EMW) absorbers of great interest among researchers. The characteristics of an ideal EMW absorber should be lightweight, thin, strong and capable of absorbing the EMW in a broad frequency range. Recently, carbon-based materials such as carbon nanotubes (CNTs) have gained good popularity for their unique properties including lightweight, high mechanical strength, good electrical and thermal conductivity and wide frequency bandwidth. However, carbon nanotubes are very conductive and tend to agglomerate due to the van der Waals forces. Therefore, the incorporation of CNTs into polymer helps to improve the EMW absorption mechanism. This research focuses on fabricating electromagnetic wave absorbers with nanocomposite based on CNT/PLA filament for additive manufacturing (3D printing). Polylactic acid (PLA) with different weight percentages of CNT fillers (1, 3, 5 wt%) was extruded to fabricate a composite filament of a diameter of 1.75 mm. The results show that different percentages of CNTs fillers have a significant effect on the morphological and crystallographic phase structure, Raman scattering and EMW absorption properties.

1. Introduction

Electromagnetic interference (EMI) pollution has become a threat and severe issue to human health such as cancer which arises from the interference of various electromagnetic waves, either internal or external as reported by Batool *et al.,* [1]. Prolonged exposure to EMI pollution not only affects the biological environment but also interferes with electronic performance resulting in signal disruption and dysfunction as reported by several authors [2,3]. Therefore, the lightweight electromagnetic wave (EMW) absorber has aroused attention for limiting EMI pollution and protecting human as well as electronic systems as also reported by several authors [4,5].

* *Corresponding author.*
E-mail address: fadzidahmohdidris@usim.edu.my

https://doi.org/10.37934/armne.19.1.8698

In the last few years, electrically conductive metals are the most often used materials for EMW absorbers due to their strong conductivity as reported by Zhang *et al.,* [6]. However, Lee *et al.,* [7] and Jiang *et al.,* [8] reported that the use of metal and metal composites is hindered by their limitations such as high density, corrosion and expensive. To overcome this limitation, the advanced EMW absorber is now mainly focused on carbon nanocomposite material for its unique structure and properties. Carbon nanostructures such as carbon nanotubes (CNTs), carbon black and graphene have gained popularity over metals because of excellent electrical conductivity, flexibility and corrosion resistance.

Among them, CNTs have great potential to be used as excellent EMW absorbers as reported by an author [9]. For instance, a 3D nitrogen-doped reduced graphene oxide/multi-walled carbon nanotubes (NRGO/ MWCNTs) composite aerogels by a facile hydrothermal and lyophilization two-step strategy was fabricated and reported by Shu *et al.,* [10]. They found that the composite aerogel with a filler content of 15 wt% displayed a minimum reflection loss of −53.3 dB at 6.5 GHz (C band) and broad absorption bandwidth of 5.2 GHz (from 11.1 to 16.3 GHz) under a small matching thickness of merely 2.0 mm. On the other hand, Chen *et al.,* [11] reported that the fabrication of MWCNTs/SiC nanocrystals/amorphous SiOC ceramic composites via a pyrolyzed process exhibited a great microwave-absorbing behaviour with the minimum reflection loss (RL) of −61.8 dB and effective absorption bandwidth (EBA) of 2.6 GHz (a thickness of 2.19 mm) at X-band.

Nevertheless, CNTs have a drawback in a massive production yield with low-cost material. The synthesis process is still restricted to carbon arc discharge and laser ablation which results in less production. Apart from increasing the quantity of CNTs production by using the chemical vapor deposition (CVD) process, incorporating CNTs with polymer is one of the promising ways to overcome this limitation that requires only less amount of CNTs as a filler in the composite as also reported by several authors [12,13]. According to Shahapurkar *et al.,* [14], polymer-based materials (such as polylactic acid (PLA), Acrylonitrile Butadiene Styrene (ABS), polycarbonate (PC), etc have the potential to attenuate the electromagnetic waves mainly by absorption, which has made them more popular in various applications, such as in civic and military technology as reported by several authors [15,16]. PLA is a biodegradable polymer used as an alternative polymer resin for composite materials due to their remarkable features such as high tensile strength, sustainability, low melting point and adaptability in many applications [17,18]. Sherwani *et.al.,* [19] reported on the effects of combining different natural fiber reinforced PLA composites giving various properties of the entire natural fibre composites.

Moreover, there are a lot of previous studies on the EM absorption properties of CNT/polymer that are being produced using various methods and sources, and according to Chen *et al.,* [20], CNTs have several benefits, including a high dielectric loss, outstanding thermodynamic stability, and low-density EM. Even so, CNTs combined with a variety of materials demonstrated a better capacity to absorb EM waves than a CNTs alone.

The CNTs is tailor-made to maximize its absorption capacity of electromagnetic waves by integrating it in a polymer matrix as an efficient technique to produce composite absorbers. An ideal EM wave absorber would have several benefits, such as high absorption efficiency, a wide absorption bandwidth, low density, and thin material thickness. However, the high material thickness and a limited effectiveness to absorb significant broadband have restricted other applications of CNTs polymer composites. Numerous significant works have already been completed to address these issues. Among these, one of the most efficient methods is to build a multi layered and porous structure. There is no question that a porous or hollow structure can reduce composite density while improving the absorption behaviour by raising the multi-reflecting and scattering percentage. The multi layered structure was shown to be effective in terms of achieving the impedance matching

requirement as reported by Kim *et al.,* [21]. Therefore, this research highlights on the preparation of low-cost CNT by using industrial waste as catalyst to synthesize multiwalled carbon nanotubes (MWCNT). It is further fabricated in filament form in order to 3D print according to the desired size and shape.

1.1 EM Absorption Mechanism

EM materials have the ability to reflect, absorb, and transmit EMW when they are emitted. Note that the term "absorption" mostly relates to the ability of EM energy to be converted to heat via intrinsic magnetic or dielectric loss. In general, according to Chen *et al.,* [20], the mechanisms of EMW absorption of CNTs-based composites are related to impedance matching and attenuation principle.

EMW absorption occurs when most of the EMW signal must be penetrating inside the absorbing material. When the incident EMW reaches the surface of the loss materials, the EMW entering the absorbers must be attenuated as much as possible. Meanwhile, the absorptivity of absorbers is related to the parameters of the relative complex permittivity ($\varepsilon_r = \varepsilon' - i\varepsilon''$) and the relative complex permeability ($\mu_r = \mu' - j\mu''$). Here, the real part (ε' and μ') relates to the energy storage capacity, while the imaginary part (ε'' and μ'') is related to the energy dissipation. As per transmission line theory, the reflection loss (RL), can be calculated using the following Eq. (1) and Eq. (2) which contribute to almost half of the absorption effect [22]

$$Z_{in} = Z_o \sqrt{\mu_r/\varepsilon_r}\tanh[j(2\pi f d/c\sqrt{\varepsilon_r \pi_r}\ )] \tag{1}$$

$$RL\ (dB) = 20\log\left|\frac{(Z_{in} - Z_o)}{(Z_{in} + Z_o)}\right| \tag{2}$$

The input impedance in this case is Z_{in} and Z_o is impedance of free space. While ε_r and μ_r are relative complex permittivity and relative complex permeability respectively. On the other hand, f stands for the incident wave frequency, c for the speed of light and, d for the thickness of EMW absorption sample.

From theoretical standpoint, an ideal impedance match can be obtained when the values of ε_r and μ_r are very close, that is, the value of $|Z_{in}\ /\ Z_o|$ near to 1. This way, the incident wave passes completely through the absorbers without reflection which resulting in an ideal reflection loss. Thus, Zhang *et al.,* [23] reported that the incident EMW permeates into absorbents completely without reflection, and the corresponding refection loss will be optimal.

Once an incident EMW penetrated the lossy material, its ability to attenuate the EMW became a critical indicator of how well it could absorb the energy. The following equation can be used to obtain the attenuation capability, which is called the attenuation constant (α) and can describe the intensity of absorption in Eq. (3) as reported by Green and Xiabo [24]

$$\alpha = \frac{\sqrt{2}}{c}\ \pi f\sqrt{(\varepsilon''\mu'' - \varepsilon'\mu')\ +\ \sqrt{(\varepsilon''\mu'' - \varepsilon'\mu')^2 +\ (\varepsilon'\mu''+\varepsilon''\mu')^2}} \tag{3}$$

Where, ε' and μ' are respectively denote as the real permittivity and real permeability. Whereas ε'' and μ'' represent the imaginary part for both permittivity and permeability respectively.

In addition, according to Liu *et al.,* [25], the ratio between the imaginary and real parts of permittivity, or the dielectric loss tangent ($\tan\delta_\varepsilon$) based on the following equation, Eq. (4) can be used to determine the dielectric loss

$$\tan \delta_{\varepsilon} = \frac{\varepsilon''}{\varepsilon'} \quad (4)$$

Dielectric loss basically refers to the attenuation of EMW that result from contact with absorbers. In other words, absorbers respond to an applied oscillating EM field to convert energy from their electric field form to their thermal form. The main components of dielectric loss are conductivity loss and polarisation loss. Polarisation loss is primarily caused by ionic, electronic, interfacial, and dipole orientation polarisation. The numerous surface atoms, unsaturated bonds, and dangling bonds of CNTs used as fillers in EM absorbers, exhibit interfacial polarisation and multiple EMW scattering. These are typical techniques for EM attenuation in composite absorbers and are crucial to the EM absorption mechanism of CNTs according to Chen *et al.,* [20].

2. Methodology

2.1 Material's Preparation

PLA pellets with 98 % of L-lactide (trademark Luminy® LX575), were purchased from Total Corbion PLA (Thailand). The density and melt flow index were 1.24 g/cm^3 and 7 g/10 min (210 °C/2.16 kg). This grade has a glass transition temperature (T_g) of 60 °C and a melting temperature (T_m) of 165 °C. PLA pellets were dried in the oven at 40 °C for 3 hours to remove moisture.

In this study, CNTs were synthesized from a mill scale waste via CVD method which mill scale as a catalyst, ethanol as a carbon source and argon gas as a carrier gas. The mill scale was first crushed for 8 hours with high energy ball milling (HEBM) to obtain smaller starting particle size. 0.1 g of mill scale was loaded into the alumina boat and placed in the furnace for CNTs growth. The temperature of the furnace was raised from room temperature to 700 °C at a rate of 5 °C/min within 2 hour 20 minutes. During the reaction, ethanol was introduced for 30 minutes while the deposition temperature was maintained. Finally, the furnace was let to cool down before the whole system was turned off. The resulting synthesized CNTs were kept in a vial for further measurement and characterization. The synthesized CNTs produced by CVD method with an average diameter size of 163.1 nm were further used.

2.2 Fabrication of CNT/PLA Filament for 3D Printing

The filaments were prepared with Siemens Twin Screw Extruder (ratio length, L over diameter, D, L/D= 24). At first, CNTs with different weight percentages (0, 1, 3, 5 wt%) were added into PLA polymer and manually mixed as shown in Table 1. 500 g of CNT/PLA mixture was inserted into the feeder gradually to avoid clumping during the melting process. There were three heating zones correspond to the feed zone, melting zone and melt processing zone and the temperature was fixed around 180-190 °C respectively. Meanwhile, the screw speed was set at 10-12 rpm. At the die, the extruded strand of the CNT/PLA composite was cooled down in a water bath and passed through a spooler to produce a uniform diameter size of the filament wire (1.75 ±0.1 mm).

Table 1
Percentage weight of CNTs

Weight % of CNT 8h	Mass CNT/PLA (g)
0%	500
1%	
3%	
5%	

After the extrusion stage, the filament was printed by using FlashForge Creator Pro 2 FDM 3D printer. The 3D model of a flat square with various thicknesses (1, 2, 3 mm) was designed using TinkerCAD software and exported as STL file format. The dimension of the 3D model refers to the waveguide size as shown in Table 2. The filament was fed into a 0.4 mm diameter nozzle. The parameter of the FDM 3D printing process was set as follows: the nozzle temperature (210 °C), bed temperature (40 °C), layer height (0.18 mm), infill density (100 %), printing speed (60 mm/s); these variables were kept constants for all models.

Table 2
Dimension of 3D printed model

Waveguide name (EIA standard)	Frequency band	Inner dimensions of waveguide opening (mm)	Thickness of 3D model (mm)
WR112	7.05 to 10 GHz	28.4988 x 12.6238	1,2,3
WR75	10.00 to 15 GHz	19.05 x 9.525	1,2,3

2.3 Materials' Characterization

The X-ray diffraction (XRD) was measured by using an X-ray diffraction (XRD, Rigaku MiniFlex 600) instrument with Cu K radiation operated at maximum power 600 W (40 kV- 15 mA). The morphology and microstructures were characterized by a field emission scanning electron microscope (FESEM, JSM-IT800 Schottky) and a high-resolution transmission electron microscope (HRTEM, FEI Tecnai G2 20 S-TWIN) respectively. The Raman scattering was characterized by using Raman Spectroscopy (Horiba XploRA PLUS). For the EM measurement, a vector network analyzer (VNA, Agilent PNA N5227A) was used to measure the scattering parameters (S-parameters) in 7 GHz – 15 GHz. Figure 1 shows the whole process scheme of 3D printed model.

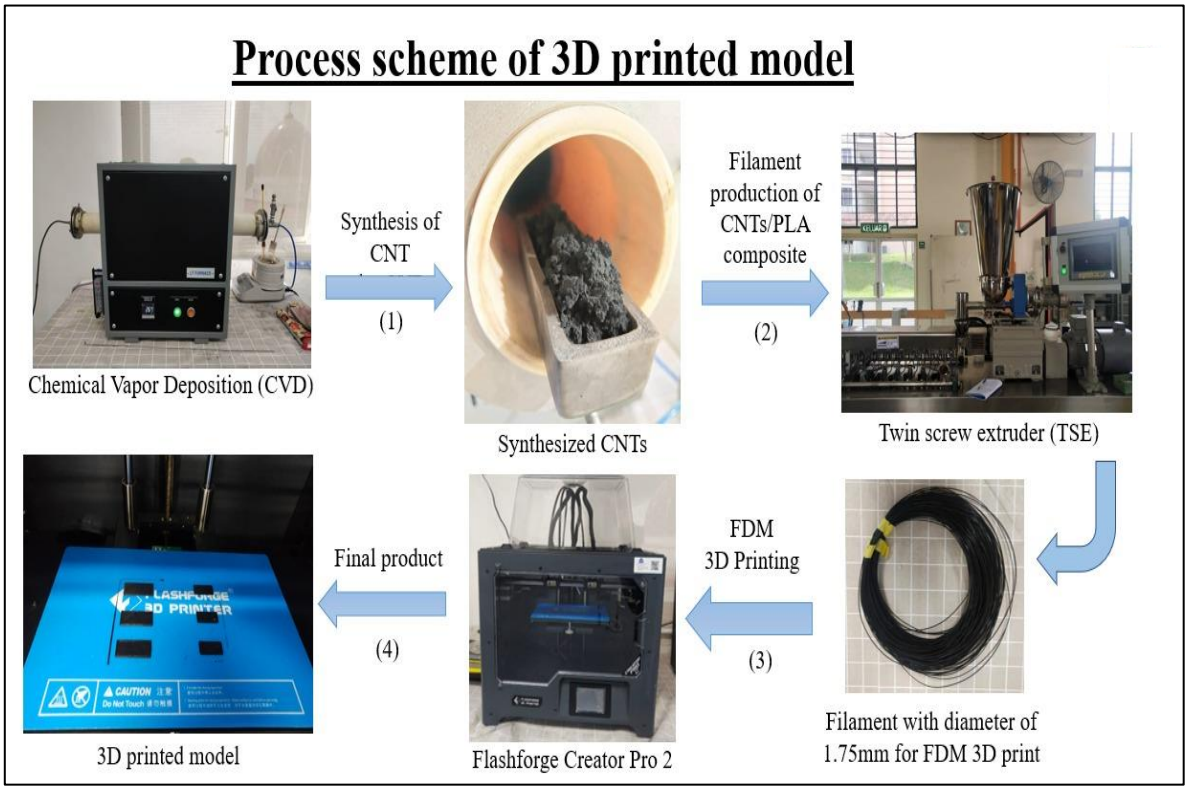

Fig. 1. Process scheme of 3D printed model

3. Results and discussion

3.1 Morphological and Particle Size of Synthesized CNTs

The surface morphology of the mill scale was analyzed based on FESEM results. Figure 2 shows the image of raw mill scale waste and Figure 3 shows the mill scale milled for 8 hours. They present a slightly similar morphology but differ in terms of particle size. The average particle size of mill scale milled at 8 hours is 278.4 nm meanwhile the particle size of raw mill scale waste is 415.5 nm respectively. The milling time is believed to be the cause of the size reduction as reported by Ruhiyuddin *et al.,* [26]. On the other hand, Figure 4 shows and revealed that the CNTs are highly entangled with each other. The average diameter of synthesized CNTs 8h is 163.1nm. The structure of CNTs was typically straight, twisted and have a high tendency to form a bundle and entanglement due to the Van der Waals interaction as reported by Mostafa *et al.,* [27]. Furthermore, the average diameter of CNTs is decreased compared to the average particle size of mill scale milled at 8 hours. This commonly happens after the production giving the lower volume fraction of the CNTs. As reported by Idris *et al.,* [28], the diameter formation of the synthesized MWCNTs was controlled by the size of the catalyst particles. Synthesized MWCNTs have a lower diameter because of decreased catalyst particle size.

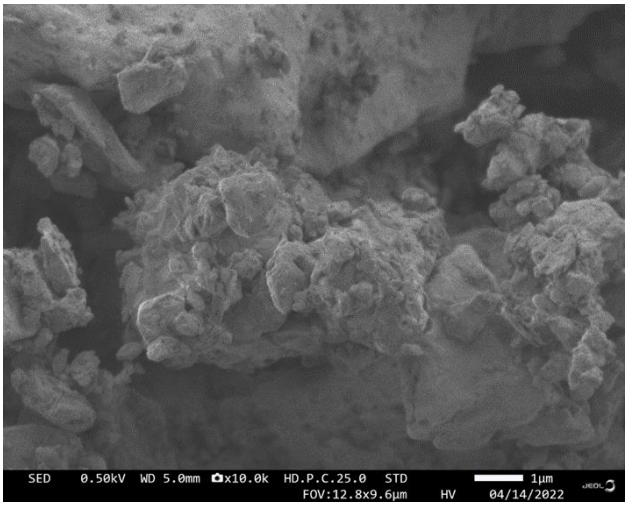

Fig. 2. FESEM image of raw mill scale waste

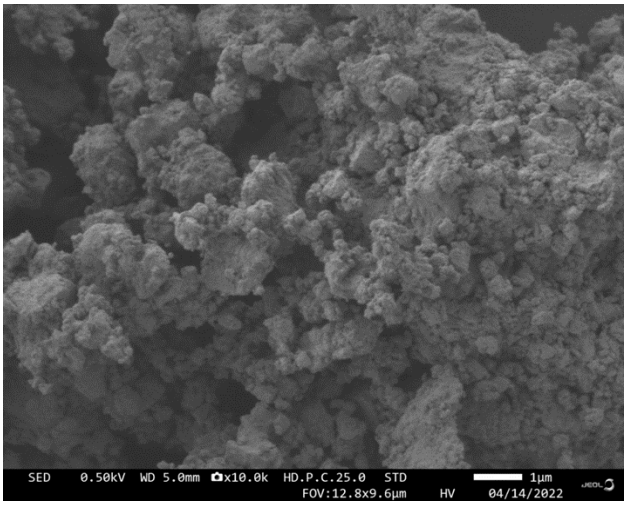

Fig. 3. FESEM image of mill scale milled for 8 hours

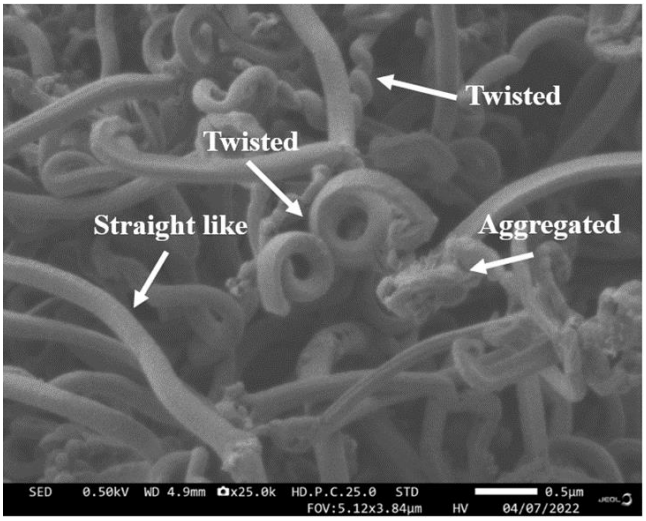

Fig. 4. FESEM image of synthesized CNTs (mill scale milled for 8 hours)

3.2 X-ray Diffraction Analysis

The crystallinity and phase analysis of CNTs and mill scale was observed by XRD as shown in Figure 5.

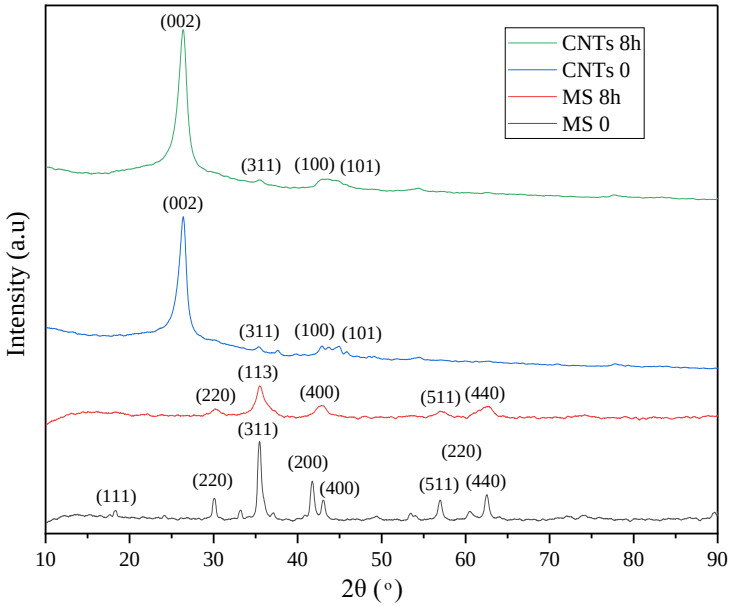

Fig. 5. XRD spectra of raw mill scale (MS0), mill scale milled at 8 hours (MS 8h), synthesized CNTs 0 and synthesized CNTs 8h

In general, mill scale is comprised primarily of wustite (FeO) and magnetite (Fe_3O_4). The results from XRD confirmed that the main phase for the raw mill scale is magnetite (Fe_3O_4) and wustite (FeO). However, for the sample mill scale milled at 8 hours, wustite peaks disappeared and showed only the presence of magnetite. As seen from the patterns, the XRD peaks for the sample raw mill scale corresponded to the diffraction pattern characteristic of the magnetite structure with (JCPD: 00-019-0629) observed at the 2θ(°) = 18.270°, 30.095°, 35.423°, 43.053°, 56.944°, 62.516° indicate to (111), (220), (311), (400), (511), (440) respectively and wustite at 2θ(°) = 41.928° (200) and 2θ(°) = 60.766° (220) with reference code (JCPD: 00-006-0615). This formation of iron oxide on the surface of the mill scale commonly occurs during the hot rolling process involving a high temperature as also reported by Ruhiyuddin *et al.,* [26].The intense peak at 2θ(°) =26.382° of CNTs represents the characteristic graphitic peak formed by the tubular structure of the carbon atoms in the sample with (002) planes with the reference code data (JCPD: 00-041-1487). Considering the spectral profile of CNTs, the weak broad XRD peak at 2θ = 42.402° and 2θ = 44.600° with (JCPD: 00-023-0064) is assigned to graphitic (100) and (101) crystalline lattice that related with Bragg law. In addition, the presence of magnetite (Fe_3O_4) can be seen at 2θ = 35.423° in the plane (311) with the reference code (JCPD: 00-019-0629). The (002) peak of CNTs 8h and CNTs 0 shows an increase FWHM pattern intermediate between amorphous carbon and crystalline due to the smaller size particle of CNTs. Singh *et al.,* [29] reported that the smaller the size of particle the greater the value of FWHM and the peak shift will broaden as the FWHM value increase, and these properties indicate higher EMW absorption than crystalline CNTs.

3.3 Elemental Analysis

The elemental composition of synthesized CNTs of mill scale milled for 8h was detected with an Energy-Dispersive X-ray (EDX). Figure 6 illustrates the presence of oxygen (O), copper (Cu), iron (Fe) and carbon (C) peaks. The appearance of a high carbon peak is from the production of CNTs and the presence of iron (Fe) due to the use of mill scale as a catalyst. Meanwhile, the existence of the element copper (Cu) was due to the sample preparation for the characterization involving a copper grid.

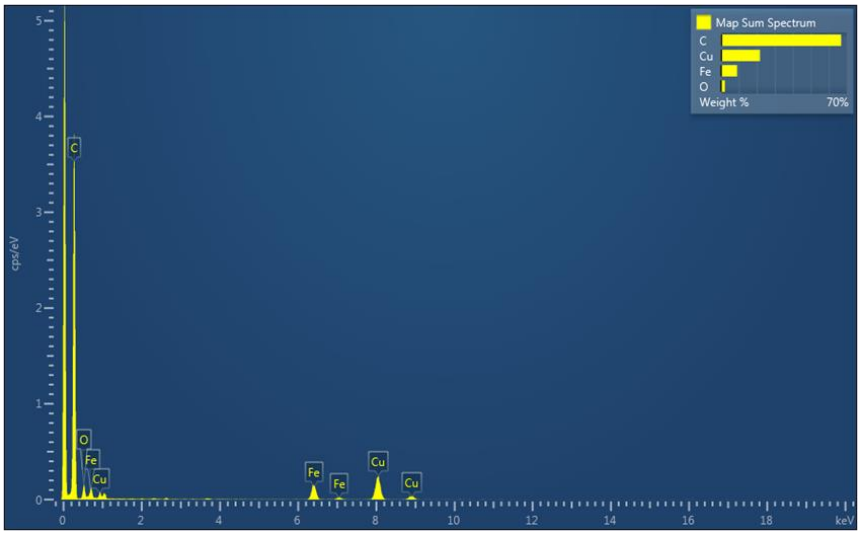

Fig. 6. EDX pattern of synthesized CNTs 8h

3.4 HRTEM

High-resolution TEM (HRTEM) image of synthesized CNTs 8h exhibits layers of conductive tube walls in a uniform arrangement as shown in Figure 7(a). The average external diameter of CNTs 8h is 90.027 nm while the internal diameter is 39.074 nm. Figure 7(b) shows the coaxial cylindrical layers with a d-spacing of 1.4Å. The wall thickness of CNTs is 25.4765 nm which produces 176.9201 layers of carbon nanotubes.

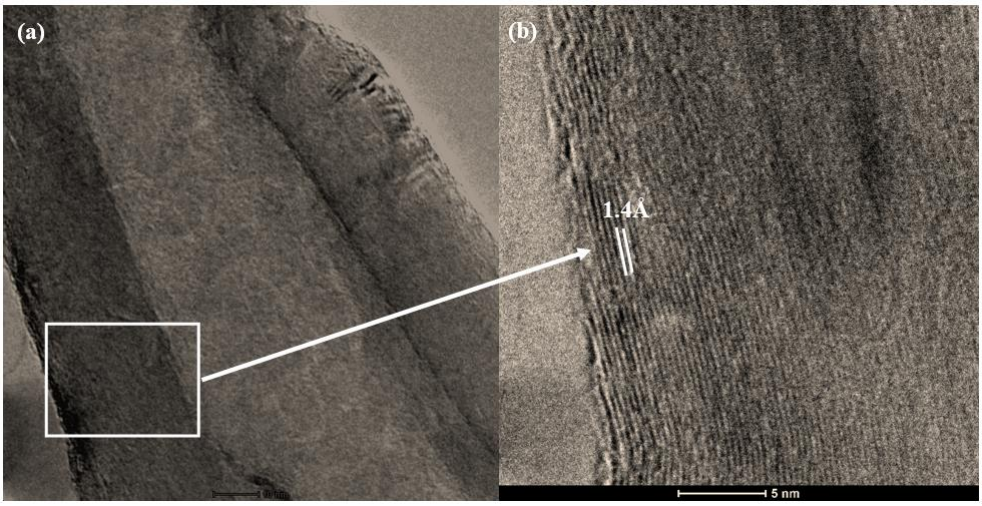

Fig. 7. a) HRTEM image of synthesized CNTs 8h b) Enlarge image of the tubular structure of CNTs 8h

According to Singh *et al.,* [29], MWCNT comprises two or more concentric cylindrical shells that coaxially form around a central hollow core due to the van der Waals forces, with an average spacing of 0.34 nm, similar to graphite. MWCNTs have an external diameter of 5-50 nm and a length of 100 nm to several centimetres. The multi-layer structure of CNTs indicates the excellent absorption of EMW due to the multiple reflections between the layered interfaces as reported by Zhao *et al.,* [30].

3.5 RAMAN Scattering

The vibrational mode and Raman spectra of synthesized CNTs 8h are illustrated in Figure 8. The Raman spectrum has two major peaks known as D-band and G-band. Su *et al.,* [31] reported that, D-band represents a defect in the graphitic structure that is caused by out of plane vibration form at around 1335 cm^{-1}, whereas the G-band is caused by in plane vibration of the C-C bond from the sp^2 orbital indicate graphitic structure form at around 1570 cm^{-1}. The ratio of I_D/I_G was used to identify the degree of graphitization and defect density.

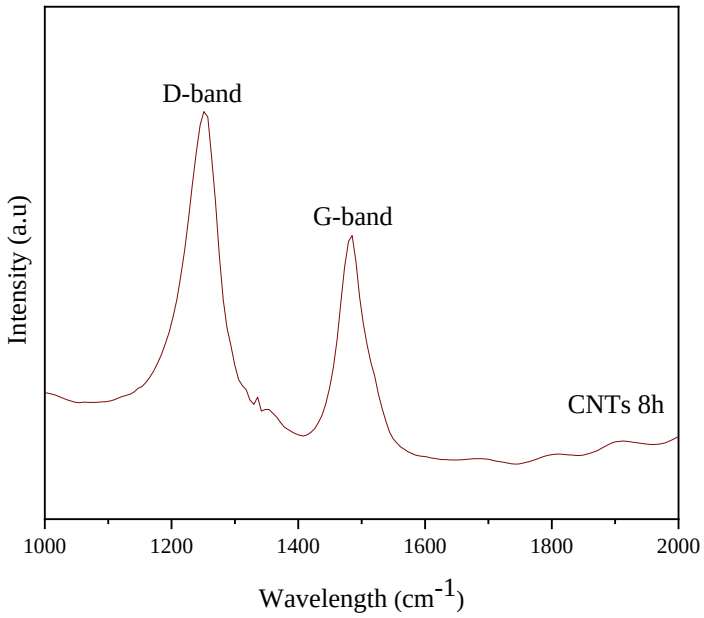

Fig. 8. Raman spectrum of synthesized CNTs of mill scale milled at 8 hours

Based on Figure 8, result of the intensity ratio of I_D/I_G is 1.3010 which suggested that the CNTs have a high defect density and lower graphitization. The presence of defects in the structure is desirable because it shows a lower conductivity helping in an EMW absorption performance. Thus, the higher D-band also shows that it was related with the production of more multi-walled CNTs compared to single-walled CNTs.

3.6 EM Absorption Performance

This study measures the EMW absorption coefficient in three sets of samples of different CNTs thicknesses. Each thickness of CNTs has different filler's percentages of 0%, 1%, 3% and 5% filler weight percentages of CNTs in the range of frequency from 7 GHz to 15 GHz as shown in Figure 9.

As microwave energy penetrates a lossy dispersive material which in this case CNT/PLA composite, EM field interactions with the substance's molecular and electronic structures. In

addition, microwave radiation's energy is partially reflected, absorbed, and transmitted when it penetrates a solid surface. Transmittance (T), reflectance (R), and absorbance (A) can be computed using the formula in Eq. (5)-(7), according to the analysis of S-parameters by Nwigboji *et al.,* [32]

$$T = |S_{12}|^2 = |S_{21}|^2 \quad (5)$$

$$R = |S_{11}|^2 = |S_{22}|^2 \quad (6)$$

$$A = 1 - R - T \quad (7)$$

Where the scattering parameters of the two port network systems, S_{11} or S_{22} and S_{12} or S_{21}, represent the reflection coefficient and transmission coefficient.

Based on Figure 9(a)-(c), there are fluctuations in each of the absorption coefficient graph with several high peaks and low peaks. In Figure 9(b), there are four obvious high peaks for samples with 2 mm thickness. The highest absorption coefficient peaks for all CNTs percentages occurred at the frequency range of 7 GHz to 8 GHz with the absorption coefficient value of 0.81 (CNT 0%), 0.77 (CNT 1%), 0.79 (CNT 3%) and 0.8 (CNT 5%). Another high peak occurred at the frequency between 9 GHz to 10 GHz with the coefficient value of 0.72 (CNT 0%), 0.73 (CNT 1%), 0.727 (CNT 3%) and 0.725 (CNT 5%). While the other two high peaks occurred at 12 GHz to 13 GHz and 13 GHz to 15 GHz. There is also lowest peak of absorption coefficient at the frequency range from 8 GHz to 9 GHz with CNTs 1% has the lowest absorption coefficient value of 0.62.

The highest absorption peak occurred in the frequency range 7-8 GHz for all thickness and CNTs percentages. Meanwhile, the lowest absorption coefficient peak for all thickness and CNTs percentages happened at the frequency range of 8 GHz to 9 GHz except for sample CNTs 1% with 1 mm thickness, where the lowest peak occurs at 10.3 GHz with absorption coefficient value of 0.6.

From Figure 9(a)-(c), the overall peak shift trend between the thickness of sample and the absorption coefficient peaks. The peaks absorption coefficient has a slight change of peaks position to the left as the thickness increases. For an instance, in Figure 9(c)-(c), the highest absorption peak for CNTs 1% of 1 mm is 0.8 at frequency 8GHz. Meanwhile, for CNTs 1% with 2 mm and 3 mm thicknesses the highest absorption coefficient peak is at 0.77 (7.14 GHz) and 0.88 (7.29 GHz).

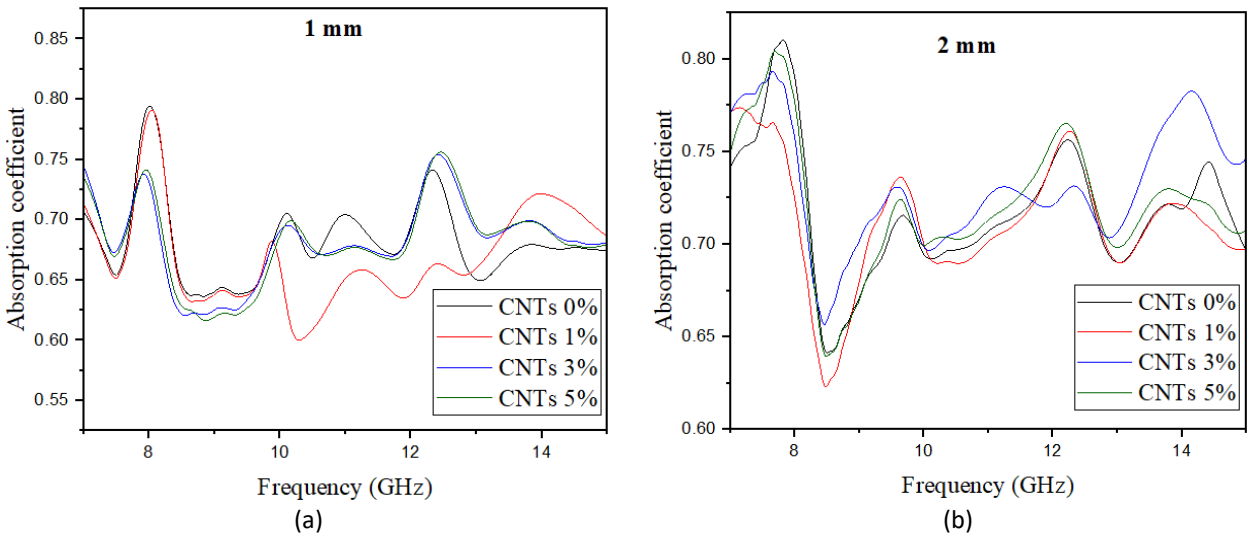

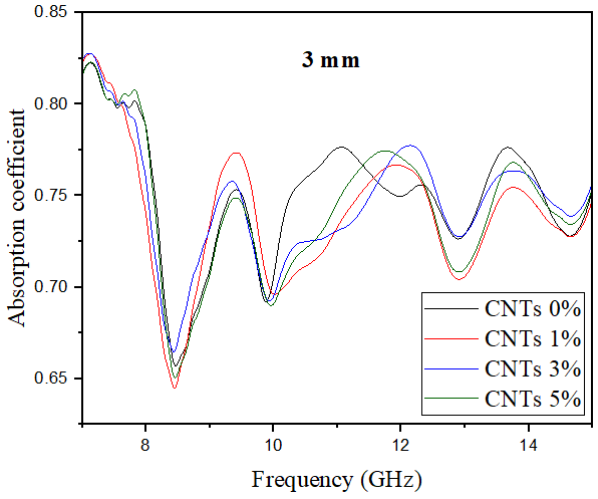

(c)

Fig. 9. Absorption coefficient graphs of different thicknesses of CNTs (a) 1 mm, (b) 2 mm, and (c) 3 mm at different filler percentages

4. Conclusions

In summary, a lightweight and low cost EMW absorber of 3D printed CNTs/PLA with different weight percentages at thickness of 1, 2 and 3 mm was fabricated by using the Fused deposition modelling (FDM) method. Different weight percentages of CNTs fillers have a significant effect on the morphological and crystallographic phase structure, Raman scattering and EMW absorption properties. Porous or hollow structure may reduce composite density while improving the absorption behaviour by increasing multiple reflection and scattering percentage. The presence of defects in the structure is desirable results in lower conductivity that helps in an EMW absorption performance. The higher D-band also shows that it was related with the production of more multi-walled CNTs compared to single-walled CNTs. Smaller particle size of the mill scale milled at 8 hours (278.4 nm) contributed to the greater value of FWHM indicated to have a high EMW absorption. Moreover, multi-layer structure of CNTs indicates the excellent absorption of EMW due to the multiple reflections between the layered interfaces. The absorption coefficient peak from the VNA result shows the fluctuation pattern in which the highest peak varies depending on the frequency. CNT 1% with thickness of 2 mm has the highest absorption coefficient peaks for all CNTs percentages occurred at the frequency range of 7 GHz to 8 GHz with the absorption coefficient value of 0.81 (CNT 0%), 0.77 (CNT 1%), 0.79 (CNT 3%) and 0.8 (CNT 5%). As the thickness increases, the absorption coefficient peak shifts towards lower frequency range.

Acknowledgement

The authors acknowledge the Ministry of Higher Education Malaysia for financial support through Fundamental Research Grant Scheme (FRGS/1/2020/STG05/USIM/02/3) (USIM/FRGS/KGI/KPT/52020) and Universiti Sains Islam Malaysia for financial support under USIM-RACER Grant (PPPI/USIMRACER_0120/KGI/051000/11920).

References

[1] Mangini, F., F. Frezza, S. Batool, and A. Bibi. "Benefits and hazards of electromagnetic waves; telecommunication, physical and biomedical: a review." *European review for medical and pharmacological sciences* (2019).

[2] Kruželák, Ján, Andrea Kvasničáková, Klaudia Hložeková, and Ivan Hudec. "Progress in polymers and polymer composites used as efficient materials for EMI shielding." *Nanoscale Advances* 3, no. 1 (2021): 123-172. https://doi.org/10.1039/D0NA00760A

[3] Tian, Ke, Danrong Hu, Quan Wei, Qiang Fu, and Hua Deng. "Recent progress on multifunctional electromagnetic interference shielding polymer composites." *Journal of Materials Science & Technology* 134 (2023): 106-131. https://doi.org/10.1016/j.jmst.2022.06.031

[4] Liang, Xiaohui, Bin Quan, Yansheng Sun, Guangbin Ji, Yanan Zhang, Jianna Ma, Daoran Li, Baoshan Zhang, and Youwei Du. "Multiple interfaces structure derived from metal–organic frameworks for excellent electromagnetic wave absorption." *Particle & Particle Systems Characterization* 34, no. 5 (2017): 1700006. https://doi.org/10.1002/ppsc.201700006

[5] Savi, Patrizia, Mauro Giorcelli, and Simone Quaranta. "Multi-walled carbon nanotubes composites for microwave absorbing applications." *Applied Sciences* 9, no. 5 (2019): 851. https://doi.org/10.3390/app9050851

[6] Zhang, Zhiwei, Zhihao Cai, Ziyuan Wang, Yaling Peng, Lun Xia, Suping Ma, Zhanzhao Yin, and Yi Huang. "A review on metal–organic framework-derived porous carbon-based novel microwave absorption materials." *Nano-Micro Letters* 13 (2021): 1-29. https://doi.org/10.1007/s40820-020-00582-3

[7] Lee, Seung Hwan, Yeongbeom Lee, Myung Geun Jang, Chonghun Han, and Woo Nyon Kim. "Comparative study of EMI shielding effectiveness for carbon fiber pultruded polypropylene/poly (lactic acid)/multiwall CNT composites prepared by injection molding versus screw extrusion." *Journal of Applied Polymer Science* 134, no. 34 (2017): 45222. https://doi.org/10.1002/app.45222

[8] Jiang, Dawei, Vignesh Murugadoss, Ying Wang, Jing Lin, Tao Ding, Zicheng Wang, Qian Shao et al. "Electromagnetic interference shielding polymers and nanocomposites-a review." *Polymer Reviews* 59, no. 2 (2019): 280-337. https://doi.org/10.1080/15583724.2018.1546737

[9] Li, Qi, Zheng Zhang, Luping Qi, Qingliang Liao, Zhuo Kang, and Yue Zhang. "Toward the application of high frequency electromagnetic wave absorption by carbon nanostructures." *Advanced Science* 6, no. 8 (2019): 1801057. https://doi.org/10.1002/advs.201801057

[10] Shu, Ruiwen, Zongli Wan, Jiabin Zhang, Yue Wu, and Jianjun Shi. "Synergistically assembled nitrogen-doped reduced graphene oxide/multi-walled carbon nanotubes composite aerogels with superior electromagnetic wave absorption performance." *Composites Science and Technology* 210 (2021): 108818. https://doi.org/10.1016/j.compscitech.2021.108818

[11] Chen, Lixin, Jia Zhao, Lei Wang, Fei Peng, Hu Liu, Jiaoxia Zhang, Junwei Gu, and Zhanhu Guo. "In-situ pyrolyzed polymethylsilsesquioxane multi-walled carbon nanotubes derived ceramic nanocomposites for electromagnetic wave absorption." *Ceramics International* 45, no. 9 (2019): 11756-11764. https://doi.org/10.1016/j.ceramint.2019.03.052

[12] Munir, Arshad. "Microwave radar absorbing properties of multiwalled carbon nanotubes polymer composites: a review." *Advances in Polymer Technology* 36, no. 3 (2017): 362-370. https://doi.org/10.1002/adv.21617

[13] Dassan, Emayaruba G. Barathi, Aslina Anjang Ab Rahman, Mohd Shukur Zainol Abidin, and Hazizan Md Akil. "Carbon nanotube–reinforced polymer composite for electromagnetic interference application: A review." *Nanotechnology Reviews* 9, no. 1 (2020): 768-788. https://doi.org/10.1515/ntrev-2020-0064

[14] Shahapurkar, Kiran, Mengistu Gelaw, Vineet Tirth, Manzoore Elahi M. Soudagar, Pavan Shahapurkar, M. A. Mujtaba, Kiran MC, and Gulam Mohammed Sayeed Ahmed. "Comprehensive review on polymer composites as electromagnetic interference shielding materials." *Polymers and Polymer Composites* 30 (2022): 09673911221102127. https://doi.org/10.1177/09673911221102127

[15] Wang, Fei, Qianfeng Zhou, Zhe Zhang, Peiwen He, Jiliang Zhang, and Kaiyong Jiang. "Microwave Absorption Performance of Carbon Black/Polylactic Acid Composite for Fused Filament Fabrication." *Applied Sciences* 12, no. 24 (2022): 12747. https://doi.org/10.3390/app122412747

[16] **吴海**华, **胡正浪**, **李雨恬**, 钱鹏, **刘力**, and **周建新**. "铁镍合金/聚乳酸复合材料的熔融沉积成形制备及其电磁吸收性能和力学性能." *Acta Materiae Compositae Sinica* 39, no. 1 (2022).

[17] Kaseem, Mosab. "Poly (lactic acid) composites." *Materials* 12, no. 21 (2019): 3586. https://doi.org/10.3390/ma12213586

[18] Bertašius, Povilas, Artyom Plyushch, Jan Macutkevič, Jūras Banys, Algirdas Selskis, Oskars Platnieks, and Sergejs Gaidukovs. "Multilayered composites with carbon nanotubes for electromagnetic shielding application." *Polymers* 15, no. 4 (2023): 1053. https://doi.org/10.3390/polym15041053

[19] Sherwani, S. F. K., E. S. Zainudin, S. M. Sapuan, Z. Leman, and A. Khalina. "Recent Development of Natural Fibers Reinforced Polylactic Acid Composites." *Journal of Research in Nanoscience and Nanotechnology* 5, no. 1 (2022): 103-108. https://doi.org/10.37934/jrnn.5.1.103108

[20] Chen, Xiaojun, Hongyang Liu, Dechao Hu, Huaqing Liu, and Wenshi Ma. "Recent advances in carbon nanotubes-based microwave absorbing composites." *Ceramics International* 47, no. 17 (2021): 23749-23761. https://doi.org/10.1016/j.ceramint.2021.05.219

[21] Kim, Jin Ah, Dong Gi Seong, Tae Jin Kang, and Jae Ryoun Youn. "Effects of surface modification on rheological and mechanical properties of CNT/epoxy composites." *Carbon* 44, no. 10 (2006): 1898-1905. https://doi.org/10.1016/j.carbon.2006.02.026

[22] Chen, Honghui, Wenle Ma, Zhiyu Huang, Yi Zhang, Yi Huang, and Yongsheng Chen. "Graphene-based materials toward microwave and terahertz absorbing stealth technologies." *Advanced Optical Materials* 7, no. 8 (2019): 1801318. https://doi.org/10.1002/adom.201801318

[23] Zhang, Hongxia, Bingbing Wang, Ailing Feng, Na Zhang, Zirui Jia, Zhengyong Huang, Xuehua Liu, and Guanglei Wu. "Mesoporous carbon hollow microspheres with tunable pore size and shell thickness as efficient electromagnetic wave absorbers." *Composites Part B: Engineering* 167 (2019): 690-699. https://doi.org/10.1016/j.compositesb.2019.03.055

[24] Green, Michael, and Xiaobo Chen. "Recent progress of nanomaterials for microwave absorption." *Journal of Materiomics* 5, no. 4 (2019): 503-541. https://doi.org/10.1016/j.jmat.2019.07.003

[25] Liu, Tong, Yu Pang, Mu Zhu, and Satoru Kobayashi. "Microporous Co@ CoO nanoparticles with superior microwave absorption properties." *Nanoscale* 6, no. 4 (2014): 2447-2454. https://doi.org/10.1039/c3nr05238a

[26] Zaki, Ruhiyuddin Mohd, Faizul Che Pa, Darus Murizam, and A. R. M. Nazri. "Study on Milling Periods on the Iron Mill Scale Particle Size and Properties." *Advanced Materials Research* 626 (2013): 1001-1005. https://doi.org/10.4028/www.scientific.net/AMR.626.1001

[27] Yusefi, Mostafa, Ong Su Yee, and Kamyar Shameli. "Bio-mediated production and characterisation of magnetic nanoparticles using fruit peel extract." *Journal of Research in Nanoscience and Nanotechnology* 1, no. 1 (2021): 53-61. https://doi.org/10.37934/jrnn.1.1.5361

[28] Idris, Fadzidah Mohd, Idza Riati Ibrahim, Farah Nabilah Shafiee, Hatika Kaco, and Mohd Shamsul Ezzad Shafie. "Materials' Properties of Lightweight Spiral Hybrid CNT/Epoxy Composites Enhanced Reflection Loss." *Journal of Advanced Research in Applied Mechanics* 113, no. 1 (2024): 13-26. https://doi.org/10.37934/aram.113.1.1326

[29] Singh, Dilip K., P. K. Iyer, and P. K. Giri. "Diameter dependence of interwall separation and strain in multiwalled carbon nanotubes probed by X-ray diffraction and Raman scattering studies." *Diamond and Related Materials* 19, no. 10 (2010): 1281-1288. https://doi.org/10.1016/j.diamond.2010.06.003

[30] Zhao, Tingkai, Cuilin Hou, Hongyan Zhang, Ruoxing Zhu, Shengfei She, Jungao Wang, Tiehu Li, Zhifu Liu, and Bingqing Wei. "Electromagnetic wave absorbing properties of amorphous carbon nanotubes." *Scientific reports* 4, no. 1 (2014): 5619. https://doi.org/10.1038/srep05619

[31] Su, Xiao, Ruoyu Wang, Xiaofeng Li, Sherif Araby, Hsu-Chiang Kuan, Mohannad Naeem, and Jun Ma. "A comparative study of polymer nanocomposites containing multi-walled carbon nanotubes and graphene nanoplatelets." *Nano Materials Science* 4, no. 3 (2022): 185-204. https://doi.org/10.1016/j.nanoms.2021.08.003

[32] Nwigboji, Ifeanyi H., John I. Ejembi, Zhou Wang, Diola Bagayoko, and Guang-Lin Zhao. "Microwave absorption properties of multi-walled carbon nanotube (outer diameter 20–30 nm)–epoxy composites from 1 to 26.5 GHz." *Diamond and Related Materials* 52 (2015): 66-71. https://doi.org/10.1016/j.diamond.2014.12.008